Study on the formability of SiCf/Ti-6Al-4V composites by fiber laying parameters and laser process parameters

RiHong Han
Jin Hao
ZhenZhong Han
FangJuan Qi
HongLi Fan
HaiQiang Yang
Haibo Qi (qhb@stdu.edu.cn)

Research Article

Keywords: TMCs, Additive manufacturing, Process parameters, Microstructure.

Posted Date: May 24th, 2022

DOI: https://doi.org/10.21203/rs.3.rs-1556499/v1

Abstract

As an important structural material for hypersonic aircraft and high thrust-to-weight ratio engines, continuous fiber-reinforced titanium matrix composites (TMCs) has high specific strength, high specific stiffness, corrosion, wear resistance and high temperature creep resistance. TMCs were directly fabricated using an additive manufacturing method that did not require a mold. The degree of fiber preservation during the preparation process and the molding quality have a signicant influence on the properties of the composite material. This paper firstly studies the effect of filament laying parameters on the forming results. This was followed by an investigation of the impact of the process parameters on the forming results using orthogonal experiments with interactions and finding out the process parameters for the best molding quality. SEM and metallographic results show that the microstructure of the composites formed under different parameters showed different amounts of martensite, columnar crystals, and equiaxed crystals. TiC was the main component of the interfacial reaction layer.

1. Introduction

The increasing speed of aircraft, higher flight temperatures, and components with more complex shapes has placed higher requirements on aircraft skin and missile tail materials [1–3]. Continuous SiC fiber-reinforced Ti-based composites have a high specific strength, high specific stiffness, and high-temperature resistance, so they have been widely used in aerospace applications and other fields. The preparation of SiC_f/Ti-6Al-4V composites using additive manufacturing methods with short production cycles and without the need for tooling and molds has unique advantages compared with traditional preparation methods such as foil-fiber-foil and powder metallurgy methods [4].

Research on additive manufacturing technologies and equipment for carbon fiber-reinforced composites has mainly focused on particle and continuous fiber-reinforced composites[5]. Particle-reinforced composite additive manufacturing mainly uses ceramic particles, carbon fibers, glass fibers, and other short-fiber materials as reinforcements. Baicheng Zhang et al.[6], Gasper et al.[7] used laser cladding deposition technology to simultaneously print and form particle-reinforced metal matrix composites. Belter et al.[8] designed cavities inside ABS specimens and filled them with high-strength resin at the end of printing to improve the strength of the printed parts. Gu Dongdong et al.[9–10] mixed metal powders with nanoparticles and used selective laser melting technology for simultaneous printing and forming, and explored a new process to prepare biocompatible materials. The method of producing particle-reinforced composites is simple, but the isotropy of the reinforcement within the matrix is poor, and the mechanical properties of the composites are only slightly improved; thus, many scholars have conducted research on continuous fiber-reinforced composites. Xiaoyong Tian et al.[11], Zhongde Shan's[12] team, and Xiao et al.[13] proposed a three-dimensional printing-based manufacturing process for continuous fiber-reinforced thermoplastic composites to realize the integrated preparation and molding of carbon fiber composites. Klift et al.[14] printed composites with different fiber percentages with the help of Mark One 3D printer from Mark Forged and conducted related mechanical experiments. The results showed that the higher the fiber content in the composites, the better their mechanical properties, but many holes

appeared inside the material. Ryosuke Matsuzaki et al.[15] developed a three-dimensional (3D) printing method for continuous fiber-reinforced thermoplastics based on fused deposition modeling, which improved the tensile strength of the composites. Existing composite additive manufacturing methods mainly use thermosetting and thermoplastic resins as the matrix materials, none of which are suitable for printing or molding continuous brittle fiber-reinforced metal matrix composites.

In this paper, laser melting experiments of continuous SiC fiber-reinforced Ti-based composites were carried out using inert forming equipment designed in-house [16–19]. In this process, SiC fibers were used as the reinforcing phase and Ti-6Al-4V as the matrix. First, fibers were laid on the titanium substrate, then the molten liquid metal titanium flowed, infiltrated, and solidified on the SiC fiber layer. Then, the fibers were repeatedly laid, and the titanium powder was melted and coated the fibers. The effects of processing parameters such as the fiber lay-up angle, fiber lay-up density, fiber lay-up arch, and process parameters such as laser power, powder feeding rate, and scanning speed on the forming results of SiC_f/Ti-6Al-4V composites were investigated. Finally, SiC_f/Ti-6Al-4V composites with completely preserved single-layer fibers and a high volume fraction were prepared. The microstructure of the SiC_f/Ti-6Al-4V composites was also studied to reveal the influence of fibers on the tissue changes and final mechanical properties. This study also provides guidance for subsequent heat treatment tests.

2. Experimental

2.1 Materials and composite fabrication

The powder used to prepare the composite was Ti-6Al-4V titanium alloy powder produced by A&P Canada, with a particle size of 45–110 μm. Before the experiment, the titanium alloy powder was dried in a vacuum drying oven at 100 ^{o}C for 2 h.

The substrate was an α + β two-phase Ti-6Al-4V titanium alloy produced by Anxi Baotian. The titanium substrate was cut into square plates with dimensions of 100 mm×100 mm×6 mm using an EDM wire cutter. The plates were mechanically polished to remove surface oxidation, cleaned by alcohol scrubbing, and put into an Ar inert chamber forming platform.

The SiC fiber was a W-core silicon carbide fiber provided by the Institute of Metals, Chinese Academy of Sciences, with a diameter of about 110 μm and a tensile strength of about 3800 MPa. The SiC fibers were put into the bearing tray of an automatic winding tray by a winding device and then stored in a storage mechanism. Finally, they were laid into a fiber layer on the titanium substrate using a spreading device.

2.2 Experimental method and characterization

The SiCf/Ti-6Al-4V composite material forming device designed by our laboratory mainly includes: inert atmosphere chamber, laser, cladding head, fiber laying, and drawing device, and three-dimensional motion platform[17]. Among them, the fiber laying and drawing device are shown in Fig. 1, including a winding drum, a thread clamp, and a thread pressing block. The laser was an IPG-4000 fiber laser from

IPG, USA, and the single-cylinder powder feeder (DPFS-1) was developed by the Beijing Institute of Aeronautical Engineering and Manufacturing. The melting head was a four-way coaxial powder feeder from Precitec, Germany.

The composite material was cut into 10 mm × 10 mm × 6 mm specimens and then hot-mounted into resin to expose the surface to be observed. The specimens were sequentially ground, polished, etched, and observed. An Olympus GX51 optical microscope was used to observe the microstructure, forming defects, fiber preservation, etc. Scanning electron microscopy was used to assess the interfacial bonding between the fiber and matrix, the thickness of the interfacial reaction layer, and the distribution of various elements. X-ray diffractometry was used to detect the interfacial reaction products of the fiber and matrix in the specimens.

3. Results And Discussion

3.1 Influence of filament laying parameters on forming results

3.1.1 Fiber density

The fiber preservation was better when the laser melting head traveled at an angle of 90° to the fiber, but the poor bonding of the composite to the matrix (Fig. 2) was caused by the high fiber lay-up density. The SiC_f/Ti-6Al-4V composite was prepared by laser melting, and the fiber lay-up density was defined according to its principle.

$$\rho = \mathrm{N} / \left(\mathrm{L}/\mathrm{d}\right) \times 100\% \quad (1)$$

where ρ is the fiber laying density, N is the number of fibers, L is the specimen size, and d is the fiber diameter. It can be seen that a different fiber density affects the flow and infiltration of the liquid titanium metal and the solidification of the melt pool. Ultimately, this affects the surface roughness of the composite forming, the thickness of the monolayer, and the bonding between layers.

Figure 2 compares the forming effects of four fiber lay-up densities with the same process parameters, which shows that the four forming effects are different. Figure 2 (a) shows a graph of the forming effect using a too-dense fiber lay-up density, i.e., the density of fibers exceeded 100%, and there were stacked fibers with many defects, mainly large unfused holes. This occurred when the fiber density was too high and when the wettability of the fibers by liquid titanium metal was poor. The poor wettability led to an unfused region between the substrate and fiber. In addition, the mobility of the liquid metal was hindered, and the liquid metal failed to fully react with the substrate and solidify quickly, which led to poor bonding of the molten cladding layer with the substrate and the existence of many voids.

Figure 2 (b) shows the forming effect with a fiber lay-up density close to 100%. In the figure, there are only a few pores between the fibers, and the bonding between the molten clad layer and the substrate is still not ideal. This is because the fiber density is still too high, and the liquid titanium metal did not effectively penetrate the fiber layer and contact the substrate to produce metallurgical bonding.

Figure 2 (c) shows the forming effect at a fiber lay-up density of 75%. It can be seen that the overall forming effect is good, with good bonding between the molten layer and the substrate, and less matrix porosity between the fibers. This is because the spacing between the fibers is suitable, and liquid titanium metal can effectively pass through the fiber layer and react with the substrate to achieve a metallurgical bond.

Figure 2 (d) shows the forming effect using a too-low fiber lay-up density, which is about 15%. Although the bonding of the molten layer to the substrate was excellent, and there were few defects within the molten layer, there were few fibers within the molten layer, as well as fiber burnout. Due to the high temperature of the molten liquid metal, after the liquid metal reacted completely with the matrix, there was too much residual heat to promote the reaction between the liquid metal and the fibers. When the number of fibers was small, more heat was borne by each fiber, and some fibers reacted completely; thus, to ensure the volume fraction of fibers in the final formed composite and prevent the fibers from being burned, it is crucial to choose a proper fiber lay-up density.

3.1.2 Fiber angle.

The angle of laying refers to the angle between the travel direction of the laser cladding head and the fibers. The effect of different laying angles on the forming quality is mainly reflected by the different continuous heat inputs to a single fiber.

A schematic diagram of the laser cladding head traveling at 0° (parallel) to the fibers is shown in Fig. 3. At this point, the laser energy continued to act on the fibers. The cumulative temperature of the subsequently-formed fibers increased due to the previous thermal influence; thus, the fibers were subjected to different thermal inputs due to the different forming sequences. The subsequently formed fibers are subjected to more signicant heat input and more violent reactions, making them more likely to undergo interfacial reactions and undergo fiber burnout.

The forming sections of the beginning and middle parts of the same sample were taken. Figure 4 is a schematic diagram that compares the forming effects. As can be seen from the fiber preservation in Fig. 4 (a), the fibers have different proportions and sizes, and are regularly arranged alternately. As can be seen from the comparison of fiber preservation between Fig. 4 (a) and Fig. 4 (b), Fig. 4 (a) is near the beginning of the sample, where there is almost no heat accumulation and fiber preservation was relatively complete. Figure 4 (b) shows the middle part of the formed sample, where the reaction layer was thicker, and the residual diameter of the fiber was smaller due to the cumulative effect of heat. The larger the cumulative thermal effect, the higher the temperature, the higher the temperature gradient, and

the more intense the reaction between the fiber and matrix. In addition, the higher the temperature, the longer the cooling time, and the longer the reaction time. Although the solidification time of the molten pool was very short, laser deposition forming is a violent non-equilibrium reaction process, and a very small time difference will lead to completely different experimental results.

The laser cladding head traveled 90° (perpendicular) to the fibers, as shown in Fig. 5. For a single fiber, there was no cumulative thermal effect on a single fiber as it moved to the next fiber immediately after the reaction by laser irradiation. In the transverse direction, there was also no heat transfer due to the presence of gaps between fibers; therefore, in this forming method, the fibers were exposed to laser irradiation for a short time, the heat generation was low, and the reaction time and degree between the fibers and the substrate were low.

In this forming method, the fibers with the same cross-section were compared first, and there was no very significant difference in the size of the fibers in the same cross-section. There were individual fibers with slightly smaller diameters, but there was no regularity, and random errors were observed (Fig. 6). The fiber diameter measured using SEM was 97 μm, which is slightly larger than the fiber diameter at the beginning of parallel fiber-forming with a laser melting head, indicating better fiber preservation; therefore, the forming method in which the laser melting head traveled perpendicular to the fibers was more suitable for the preparation of composites.

3.1.3 Fiber camber

The presence of a fiber-laying arch will lead to different longitudinal departures between single fibers, which leads to fiber burnout due to small departures and also causes the surface of the formed specimen to be bumpy. The unevenness of the specimen surface will be cumulatively superimposed, which disrupts the formation of the next layer of the composite. The presence of a fiber-laying arch can lead to different amounts of longitudinal defocusing of single fibers, which not only leads to fiber burnout, but also to bumps on the surface of the formed specimen, which is not conducive to the formation of the next composite layer.

Figure 7 shows the macroscopic morphology of the specimens with different fiber lay-up arches. For the specimens with a non-zero lay-up arch, there were some sharp bumps on the surface, which were mainly concentrated in the middle part of the specimen, as shown in Fig. 7(a). This is because the fibers in the middle of the forming platform have the smallest radius of curvature and the largest arch, resulting in the smallest defocus amount. Under the action of a smaller out-of-focus amount and larger stress, the fibers broke and straightened, which released stress. The fibers then protruded into the air and formed sharp bumps with molten liquid metal; therefore, it is essential to avoid the arching of fibers during the forming process. When the fiber lay-up arch was adjusted to zero, the surface of the formed specimen was smooth and free of bumps, which promoted the forming of the next layer of the composite, as shown in Fig. 7(b).

3.2 Influence of laser cladding process parameters on forming results

The factors affecting the final molding effect of composite materials include the process parameters and different fiber densities, thus, to obtain a good molding effect, different fiber densities should be matched with appropriate process parameters.

3.2.1 Orthogonal experiment design

Since the laser power, scanning speed, and powder feeding rate have interactive effects on the experimental results, the combined effect of these factors and the interactions between them on the experimental results must be considered; therefore, the orthogonal table L8 (2^7) was used to design an experiment to investigate these interactions. Two levels were chosen for each factor, as shown in Table 1. The table header is designed according to the "L8 (27) two-column interaction table" and uses A, B, and C to represent the laser power, powder feeding rate, and scanning speed, respectively. The test results are also included in the table.

The specimens were formed in a single layer with an area of 20 mm×30 mm and a thickness of about 1 mm. 150 fibers were laid in each layer with a density of 75%. The forming direction was perpendicular to the fibers in the direction of travel of the cladding head. The defocusing amount was + 1 mm, and the protective gas was introduced at a flow rate of 12 L/min. After the specimens were formed, they were cooled to room temperature under an inert atmosphere before being removed for the next operation.

Table 1
Forming performance test factor level table

level	Laser power/W	Feeding rate/g·min	Scanning speed/mm·s^{-1}
1	250	2.5	6
2	300	3	10

Test number	1(A)	2(B)	3(A×B)	4(C)	5(A×C)	6(B×C)	7 Empty column	Performance Indicators
1	1	1	1	1	1	1	1	90
2	1	1	1	2	2	2	2	82
3	1	2	2	1	1	2	2	85
4	1	2	2	2	2	1	1	80
5	2	1	2	1	2	1	2	70
6	2	1	2	2	1	2	1	50
7	2	2	1	1	2	2	1	80
8	2	2	1	2	1	1	2	75

3.2.2 Analysis of experimental results

The specimen surface roughness, the number and degree of macroscopic fiber preservation, interfacial bonding, and the number of defects were evaluated. Roughness cannot be evaluated using the naked eye to distinguish bumps. 150 fibers for full score, the more the number of fiber preservation, the more complete preservation score, One point is deducted for every fiber reduce, and incomplete fiber deduct 0.5 points; Full marks are given for neat, uniform joints and uniform thickness; No defects such as unfusion and pores are given full marks. The more defects, the lower the score.

The fiber preservation is the most important test index, accounting for 60% of the weight, and the remaining two indexes each account for 20%. First, the test results were analyzed by polar difference analysis, whose results are shown in Table 2. K_i in the table is the sum of the performance indexes at level 1, k_i is the mean value of the performance indexes at level 1, and Δk is the polar difference. The main relationship between each factor and interactions between factors was determined by the size of the polar difference. From the value of the polar difference in Table 2, it can be seen that $\Delta k_A > \Delta k_{A\times B} > \Delta k_B > \Delta k_{A\times C}$; therefore, the most important factor affecting the forming is the laser power, followed by the interaction between the laser power and the powder feeding rate, and the powder feeding rate and the scanning speed.

Table 2
Table of extreme difference analysis

Projects	1(A)	2(B)	3(A×B)	4(C)	5(A×C)	6(B×C)	7 Empty column
K1	337	282	327	315	300	305	300
K2	265	320	275	287	302	297	302
k1	84.25	70.5	81.75	78.75	75	76.25	75
k2	66.25	80	68.75	71.75	75.5	74.25	75.5
△k	18	9.5	13	7	0.5	2	0.5

ANOVA was performed on the results to determine the confidence level of the experimental results and to analyze the magnitude of the effect of each process parameter and parameter interactions on the experimental results. The ANOVA results of the experimental results (Table 3) show that the laser power, powder feeding rate, the interaction between the laser power and powder feeding rate, and the scanning speed all have a great effect on the experimental results. The confidence level was relatively high (> 95%).

Table 3 Analysis of variance table

Factors	Variance sum of squares	Variance	*F ratio*	Threshold value Fα	Significance
A	68	68	*1296*	$F_{0.05}$=161.4	**
B	180.5	180.5	*361*	$F_{0.05}$=161.4	**
A×B	338	338	*676*	$F_{0.05}$=161.4	**
C	98	98	*196*	$F_{0.05}$=161.4	**
A×C	0.5	0.5	*1*	—	—
B×C	8	8	*16*	$F_{0.25}$=5.83	—
Errors	0.5	0.5	—	—	—

The optimal process parameters were derived by analyzing the extreme differences and analysis of variance, by considering the factors with the greatest influence on the experimental results first, and then selecting other factors in turn; therefore, the optimal experimental results were a laser power of level 1. The interaction between laser power and powder feeding rate was greater than the powder feeding rate alone. The powder feeding rate should consider interactions between the laser power and powder feeding rate, and its interaction in level 1 is better, corresponding to A_1B_1 or A_2B_2. Thus, the powder feeding rate should be level 1; the scanning speed at level 1 was the best. The optimal process parameters were a laser power of 250 W, powder feeding rate of 2.5 g/min, and scanning speed of 6 mm/s. The composite fibers formed under this process were well preserved, with almost no burning damage, and there were no defects in the cladding layer, as shown.

In the case of a small amount of powder feeding, the increase of laser power will increase the burning loss of the fiber, resulting in a decrease in strength; The high powder feeding rate will cause the laser energy to not be well deposited on the fiber and the matrix, so that the cladding layer cannot be well combined with the matrix, resulting in defects such as unfusion, which seriously affects its mechanical properties. The influence of scanning speed is small, but too low scanning speed will undoubtedly cause more energy to be deposited into the molten pool, resulting in serious fiber burning.

3.2.3 Microstructure analysis

By analyzing the microstructure of composite samples, it was found that the microstructure of Ti-6Al-4V powder was martensitic formed under laser deposition. It contained an incipient β phase wrapped around an acicular α' phase, as shown in Fig. 9. This organization has poor plasticity and impact toughness but good creep resistance; however, when the Ti matrix and SiC fibers were compounded, the tensile hardness, wear resistance, and creep resistance was improved, mainly because the SiC fibers played a dominant role. The introduction of fibers changed the organization, which in turn affected its properties.

Figure 10(a) shows the metallographic picture of the composite, which shows that the titanium matrix was no longer monomartensitic after deposition, but rather equiaxed crystalline away from the fibers and partially dendritic near the fibers. The formation of martensite is due to the higher melt pool temperature caused the β-phase grains to grow rapidly, forming coarse primitive β grains, and the higher cooling rate caused the precipitation of α' grain boundaries and needle-like α' at the primitive β grain boundaries. The dendrites formed because the solidification conditions of the melt pool changed after adding fibers during the solidification of the liquid melt pool. The temperature of the fibers changed because the melt head traveled perpendicular to the fibers. Columnar crystals formed due to the outward diffusion of the elements in the fibers and their reaction with the matrix.

Figure 10(b) shows an SEM image of the micromorphology of the formed specimen. Both the SEM images and metallographic results show the presence of martensite, columnar crystals, and equiaxed crystals in the microstructure. In addition, there are scattered white dendrites of different sizes, which were mainly second-phase compounds and other interfacial reaction products.

To determine the phase composition of the elements, XRD patterns were obtained for the formed SiC_f/Ti-6Al-4V composites (Fig. 11). The reaction products included TiC, Ti_5Si_3, α-Ti, β-Ti, $AlTi_3$, and SiC. Combined with the surface scan analysis, the interface products were TiC and Ti_5Si_3. Because of the presence of a carbon coating, C and Ti reacted to form TiC. It can be seen from the morphology diagram that the reaction layer boundary was very uneven, and some places had thick reaction layers because the C coating was consumed. Ti reacted with diffused Si atoms to form Ti_5Si_3.

4. Conclusion

In this paper, continuous fiber-reinforced titanium matrix composites were prepared by laser cladding technology, the influence of filament laying parameters on the forming quality was explored, and the

optimal laser cladding process parameters for fiber retention and good forming were obtained by orthogonal experiments. The microstructure and phase were analyzed by metallographic microscope, scanning electron microscope and XRD. The following conclusions were drawn from this work:

(1) When the laser melting head traveled at an angle of 0° (parallel) to the fiber, single fibers were subjected to a continuous thermal load and easily burned. When the laser melting head traveled at an angle of 90° (perpendicular) to the fiber, single fibers were subjected to a cyclic thermal load and did not easily burn. When the fiber density was low, there was less reinforcing phase in the composite. When the fiber density was high, there was aggregation and burnout between the fibers. The optimal fiber density was 75%. Under the action of thermal stress, fibers produced a laying arch that caused different amounts of defocusing from the focusing spot; therefore, the laying arch of fibers should be less than 5×10^{3}.

(2) There were interactions between the laser power, powder feeding rate, and scanning speed. Through orthogonal experiments, the optimal process parameters were a laser power of 250 W, a powder feeding rate of 2.5 g/min, and a scanning speed of 6 mm/s. The fibers in the composites formed using these process parameters were well preserved, and there were fewer defects in the molten layer.

(3) In the SiC_f/Ti-6Al-4V composite, the tissue composition was not uniform due to the presence of fibers, and equiaxed crystals existed in the matrix away from the fibers. The grains became fine near the fibers, and some grains were columnar crystals. The interfacial products were TiC and Ti_5Si_3, where TiC was the main component of the interfacial reaction layer.

Declarations

Funding This work is supported by the National Natural Science Foundation of China (Grant Nos. 51775359).

Availability of data and material All data generated or analyzed during this study are included in this published article.

Code availability Not applicable

Authors' contributions HaiBo Qi and RiHong Han designed all experiments included in this study, wrote and modified this manuscript. Jin Hao and ZhenZhong Han performed the experiments. Hongli Fan and HaiQiang Yang analyzed the data, FangJuan Qi made suggestions about this manuscript.

Declaration of interests The authors declare that they have no competing financial interests or personal relationships that could have appeared to influence the work reported in this paper.

Ethics approval The article follows the guidelines of the Committee on Publication Ethics (COPE) and involves no studies on human or animal subjects.

Consent to participate Authors agree to the authorship order.

Consent for publication All authors have read and agreed to the published version of the manuscript.

References

1. Wang YM, Zhang GX, Zhang X et al Research progress of continuous SiC fiber reinforced titanium matrix composites.2016, 52(10):1153–1170
2. Zhao B, Jiang B, Gao ZY et al (2013) Transverse strength analysis of continuous SiC fiber reinforced titanium matrix composites. Chin J Rare Met 37(3):372–377
3. Cai JM, Mi GB, Gao F et al (2016) Research and development of advanced high temperature titanium alloy materials for aero-engine. 44:1–108
4. Huang H, Wang MJ, Li H et al (2018) Preparation of SiC Fibers Reinforced Titanium Matrix Composites. 61:26–364
5. Bahl S (2021) Fiber reinforced metal matrix composites - a review. Materials Today: Proceedings, 39:317–323
6. Zhang B, Bi G, Wang P et al (2016) Microstructure and mechanical properties of Inconel 625/nano-TiB2 composite fabricated by LAAM. Mater Des 111:70–79
7. Gasper AND, Catchpole-Smith S, Clare AT (2017) In-situ synthesis of titanium aluminides by direct metal deposition. J Mater Process Technol 239:230–239
8. Belter JT, Dollar AM (2015) Strengthening of 3D printed fused deposition manufactured parts using the fill compositing technique. PLoS ONE 10(4):e0122915
9. Donghua D, Kun C, Dongdong Gu et al (2017) Microstructure evolution and mechanical properties of Al-Al_2O_3 composites fabricated by selective laser melting. Powder Technol 310:80–91
10. Zhengjie MA, Can REN, Biao YAN, Lianfeng WANG, Lingyu CHENG (2018) Preparation and Creation of the Composite of 316L Stainless Steel and CaSiO3 for Bone Repairing Implantation. Nonferrous Metal Materials And Engineering 39(1):31–37
11. Tian XY, Zhang YY, Liu TF, Li DC (2016) Interface and performance of 3D printed continuous carbon fiber reinforced PLA composites. Compos A 88:198–205
12. Shan ZD, Liu F, Yang DX et al Rapid forming method for metal matrix composite material parts. CN201410762728.8, 2014-12-14(in Chinese).
13. Xiao JianHua (2016) Extrusion of carbon fiber reinforced thermoplastic plastics for 3D-Printing. Plast Ind 44(6):46–48
14. Klift FVD, Koga Y, Todorki A et al (2016) 3D Printing of Continuous Carbon Fibre Reinforced Thermo-Plastic (CFRTP) Tensile Test Specimen. J Compos Mater 6(1):18–27
15. Matsuzaki R, Ueda M, Namiki M et al (2016) Three-dimensional printing of continuous-fiber composites by in-nozzle impregnation. Sci Rep 6:23058
16. Qi HB, Tang HC, Lin Q et al Fiber laying device and composite material additive manufacturing equipment and silk laying method. CN201810689907.1, 2018-10-19(in Chinese).

17. Haiqiang Yang H, Tang L, Hao et al (2021) Process parameters and formation mechanism of SiC_f/Ti6Al4V composites manufactured by a hybrid additive manufacturing method. J Mater Process Technol 291:117037
18. Wang WM Development of miniaturized laser cladding deposition equipment.2018
19. Tang HC (2020) Design on the equipment and research on the process parameters of laser cladding & laminated object depositon of SiC fiber reinforced titanium matrix composites.

Figures

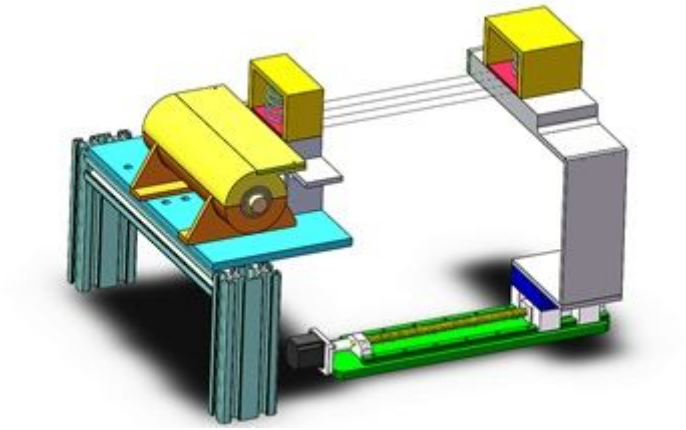

Figure 1

Schematic diagram of fiber laying and drawing device.

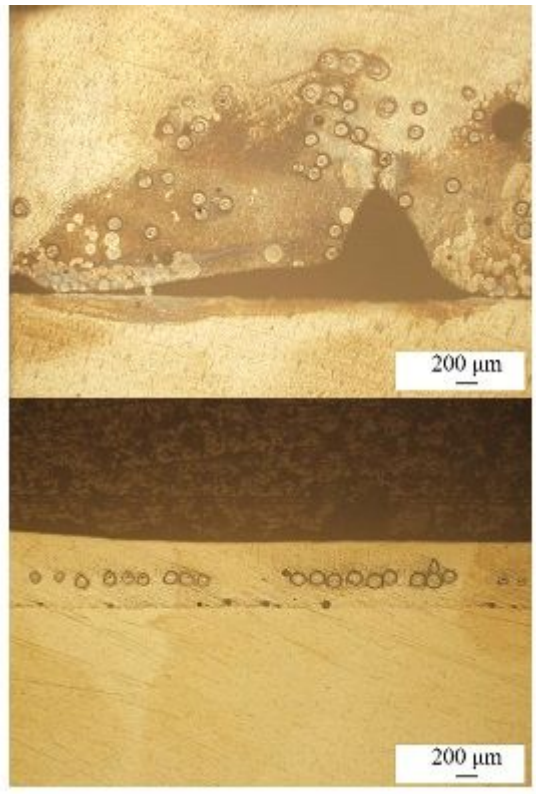

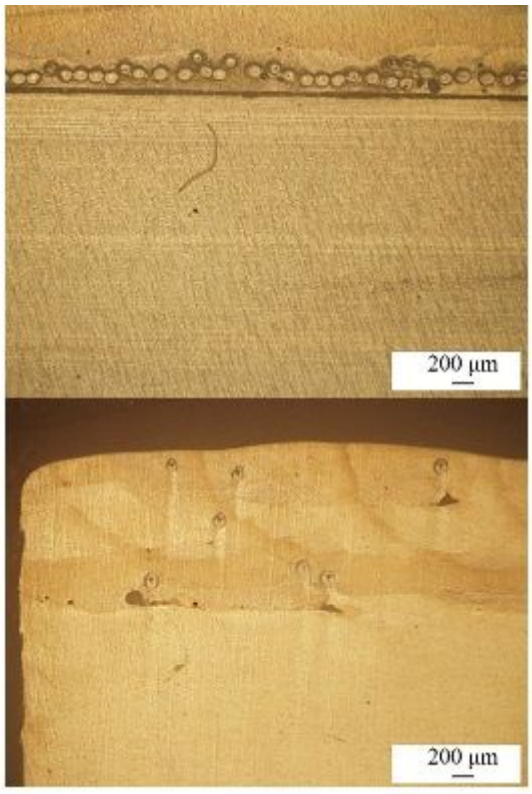

Figure 2

Comparison of forming effect of different fiber laying density. (a) Fiber density >100%. (b) Fiber density =100%. (c) Fiber density =75%. (d) Fiber density =15%

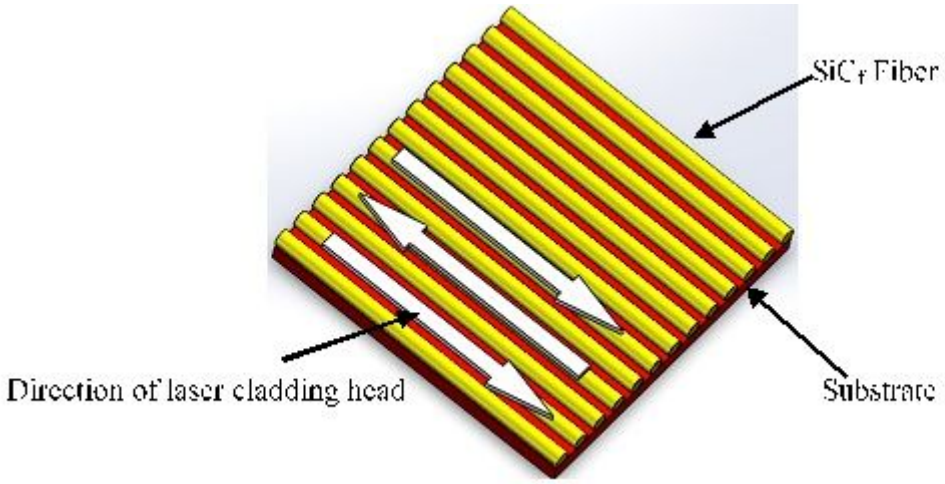

Figure 3

Scanning diagram of the laser cladding head traveling direction and fiber angle 0°.

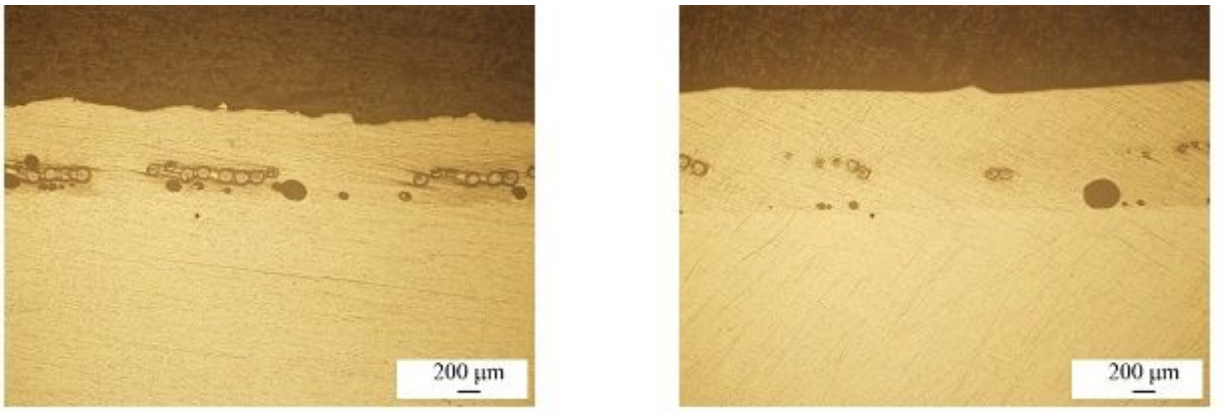

Figure 4

Fiber preservation at a nip angle of 0°. (a) Starting section of the specimen. (b) Middle section of the specimen.

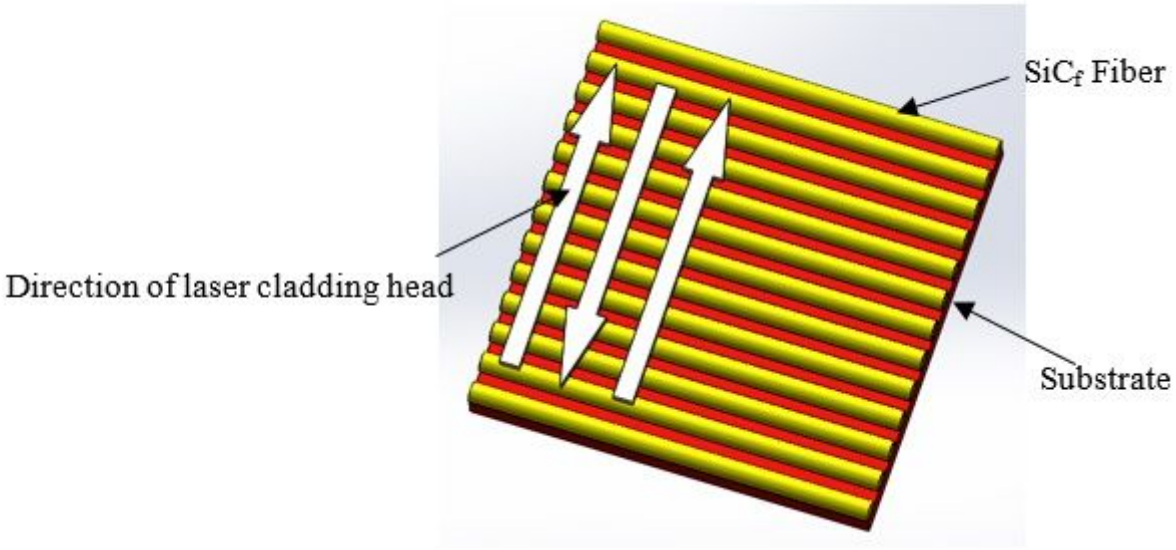

Figure 5

Scanning diagram of the laser cladding head traveling 90° to the fiber.

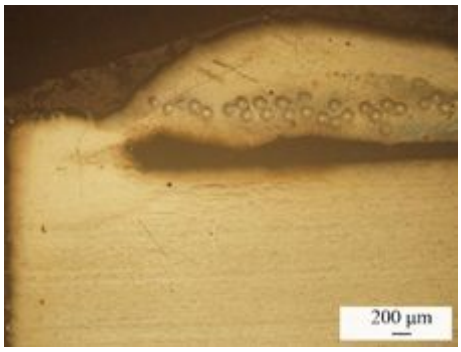

Figure 6

Fiber preservation at 90° clamping angle.

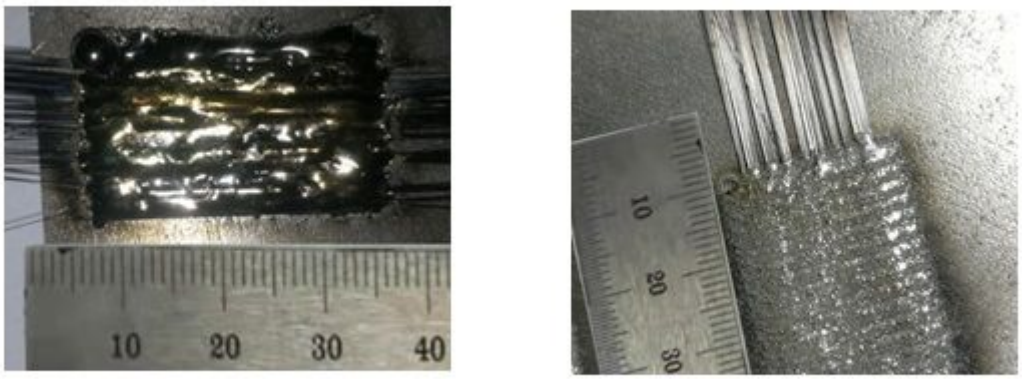

Figure 7

Appearance of forming specimens with different fiber arch. (a) Fiber laying arch is not zero. (b) Fiber laying arch is zero.

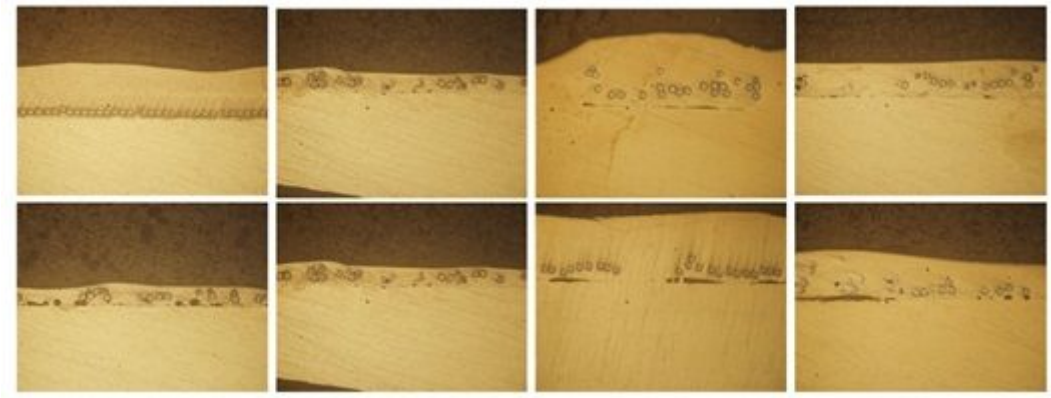

Figure 8

Single-layer optimal process forming.

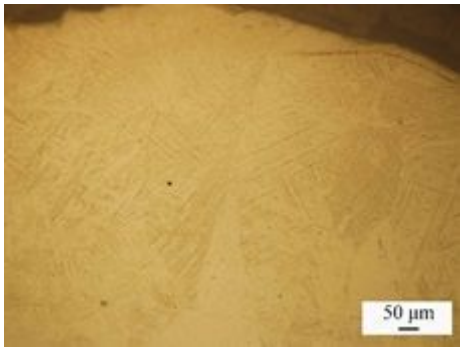

Figure 9

Ti-6Al-4V laser-cladding microstructure.

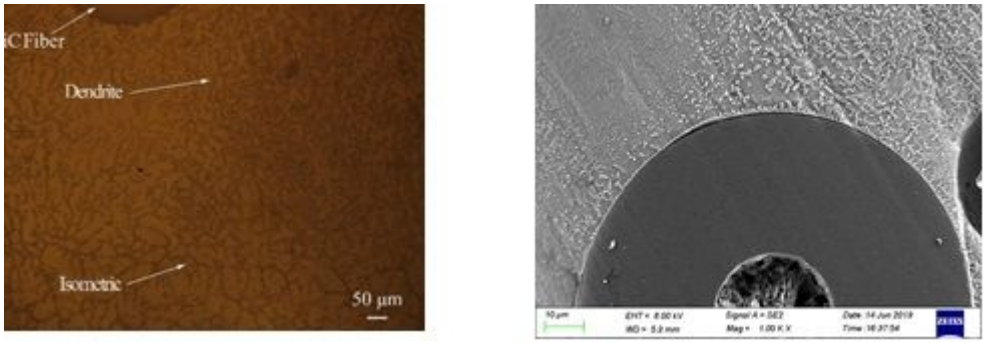

Figure 10

Microstructure near the fiber. (a) Metallographic drawing. (b) SEM images.

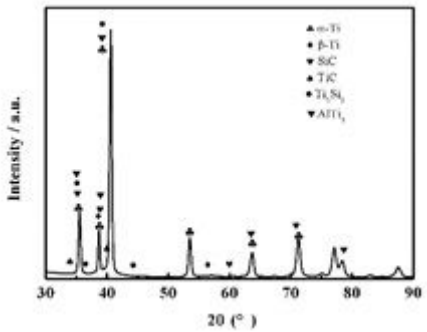

Figure 11

XRD pattern of SiC_f/Ti-6Al-4V.